

# Observation of stochastic resonance in directed propagation of cold atoms

Alexander Staron<sup>1,†</sup>, Kefeng Jiang<sup>1,†</sup>, Casey Scoggins<sup>1</sup>, Daniel Wingert<sup>1</sup>, David Cubero<sup>2</sup>, and Samir Bali<sup>1\*</sup>

<sup>1</sup> *Department of Physics, Miami University, Oxford, Ohio 45056-1866, USA*

<sup>2</sup> *Departamento de Física Aplicada I, Universidad de Sevilla, Spain*

(Dated: August 30, 2022)

A weak probe of light illuminates randomly diffusing atoms confined in a dissipative optical lattice. The probe transmission spectrum reveals directed propagation of a specific velocity-class of atoms. Resonant enhancement of this directed propagation is observed as we vary the random photon scattering rate. We experimentally characterize this stochastic resonance as a function of probe intensity and lattice well depth. A novel one-dimensional model reveals how the probe-excited atomic density waves and optical pumping rates conspire to create directed atomic propagation within a randomly diffusing sample.

Random fluctuations dominate the transport of sub-microscopic systems immersed in a noisy environment, e.g., spontaneous emission recoils in the case of resonantly illuminated cold atoms. The ability of “Brownian ratchets” to convert random fluctuations into useful directed motion is a central topic in non-equilibrium statistical physics that has been carefully explored in theory and experiment [1–3]. In particular, the phenomenon of “stochastic resonance”, which refers to a peak in system response as a function of increasing noise strength, has received wide attention in the physics community [4–6], even finding application in climate science [7], biology [8] and, more recently, in engineering [9, 10]. It has been pointed out that naturally occurring protein motors are able to power the processes of life by harnessing energy from surrounding Brownian fluctuations with efficiencies that are orders of magnitude larger than any artificial nano machine built to date [11]. Thus the notion that the controlled addition of random noise fluctuations may help rather than hinder system performance is of fundamental importance, as seen in the recent observation of stochastic resonances in quantum tunneling [12, 13], and furthermore, has potential implications for realizing efficient nano devices [14] and sensors [15, 16].

Cold atoms confined in dissipative optical potentials [17], where spontaneous emission is significant, are an ideal testbed to study stochastic resonance: The system (i.e., the confining potential) and the random environmental noise (i.e., spontaneous emission recoils, or thermal collisions) can be independently varied by adjusting beam parameters. Recently, in an elegant experiment, stochastic resonances were detected in cold atoms in a dissipative double-well potential formed by splitting a magneto-optical trap with a blue-detuned sheet of light: Random thermal collisions caused the atoms to hop between the two wells, and stochastic resonances were observed in the interwell hopping rate as a function of temperature, while also varying barrier height and atom number [18].

In this Letter, we report on the observation and experimental characterization of stochastic resonance in the directed propagation of cold atoms confined in a dissipative

optical lattice. Here, transfer between adjacent wells of the periodic potential array is caused by stochastic optical pumping processes. In previous work, stochastic resonance in a dissipative lattice was predicted [19–21], and preliminary evidence was observed by modulating the lattice potential and detecting a resonant enhancement in small center-of-mass displacements of the diffusing atom cloud [22]. In contrast, we reveal stochastic resonance via pump-probe spectroscopy, which permits a first experimental exploration of the dependence of the stochastic resonance on the lattice well-depth and the strength of lattice modulation. A new theory [23], based on the decomposition of the current into its atomic density wave contributions, elucidates how probe-modulated ground-state potentials and optical pumping rates conspire to generate resonantly enhanced directed propagation.

We consider cold atoms in a so-called 3D-lin $\perp$ lin configuration [17, 21], formed by confining the  $F_g = 1/2 \leftrightarrow F_e = 3/2$  atoms in an optical lattice created by the superposition of four red-detuned laser beams of amplitude  $\mathcal{E}_0$  and frequency  $\omega_L$ . Two beams lie in the plane  $xOz$ , with angle  $\theta_x$ , counterpropagating to the other two, which are in the plane  $yOz$  with angle  $\theta_y$ , as illustrated in Fig. 1 (a). The beams produce two light-shifted ground-state  $\pm 1/2$ -spin potentials  $U_{\pm}(x, y, z)$ , as detailed in Sec. S1 and S2 of the supplementary notes, with well-depth  $U_0$  shown in Fig. 1 (b). We focus on movement along the  $x$ -direction. A one-dimensional model arises after neglecting movement in the other perpendicular directions [19–22]. By formally considering  $y = z = 0$ , the optical potential in each ground state is given by [17, 21]

$$U_{\pm}(x) = \frac{U_0}{4} [-3 - \cos(2k_x x) \pm 2 \cos(k_x x)], \quad (1)$$

with transition probability rates between them given by

$$\gamma_{\pm}(x) = \frac{2\Gamma_S}{9} [3 + \cos(2k_x x) \pm 4 \cos(k_x x)], \quad (2)$$

where  $k_x = k_L \sin \theta_x$ ,  $k_L$  is the laser beam wave number,  $U_0 = -16\hbar\Delta'_0/3$ ,  $\Delta'_0 (< 0)$  is the light-shift per lattice field, and  $\Gamma_S$  is the photon scattering rate per lattice beam. We have checked that, within the parameter range

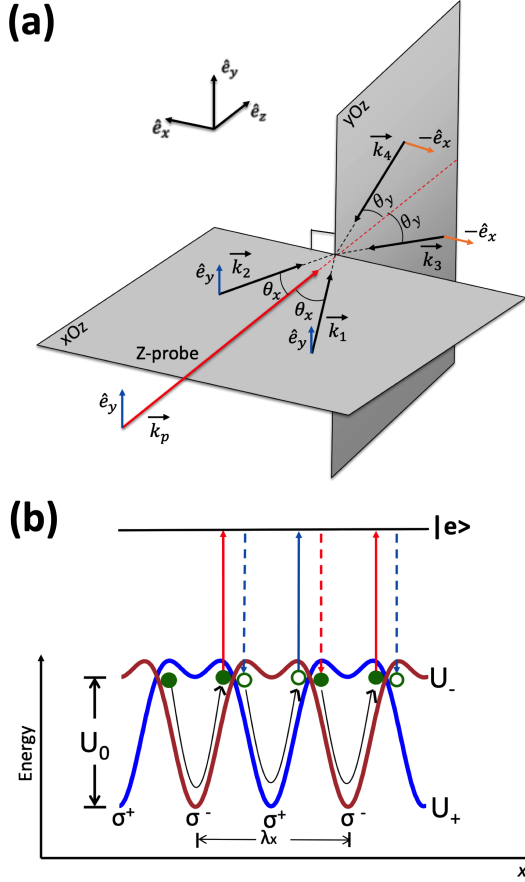


FIG. 1. (a) Scheme of the 3D tetrahedral lin $\perp$ lin lattice (b) Optical potential  $U_{\pm}$  along the  $x$ -direction ( $y = z = 0$ ) seen by a  $F_g = 1/2 \rightarrow F_e = 3/2$  atom in the above lattice, with well-depth  $U_0$  and spatial periodicity  $\lambda_x = 2\pi/k_x$ .

studied here, semiclassical [24, 25] simulations of the 3D and 1D systems provide qualitatively equivalent results.

In each ground state, atoms oscillate in optical wells with vibrational frequency

$$\Omega_X = k_x \sqrt{\frac{3U_0}{2m}} = 4 \sin \theta_x \sqrt{|\Delta'_0| \omega_r}, \quad (3)$$

where  $\omega_r = \hbar k_L^2 / (2m)$  is the recoil frequency. But this motion is not uninterrupted, the interaction with the laser also produces random absorption-emission processes with the excited states (collectively denoted by  $|e\rangle$ ). Photon scattering is viewed as noise, analogous to Brownian fluctuations in thermal systems, occasionally pumping an atom into the other ground state sublevel at the rate  $\gamma_{\pm}$  (2), and causing spatial diffusion [21]. The transitions are most likely at the peaks of the potential barriers, a distance  $\pi/k_x$  from the bottom of the well, yielding the well-known Sisyphus damping, where atoms most likely “climb hills”, continuously dissipating energy.

Since the atoms are most likely pumped to a neighboring well via sublevel transitions at the turning points in their oscillations, after half a time-period  $\pi/\Omega_X$ , the av-

erage velocity associated with this half-oscillation is given by  $v_S = \Omega_X/k_x$ . Once in the new ground state sublevel, it takes another half a period  $\pi/\Omega_X$  to reach the turning point on the other side of the well, also half a period length  $\pi/k_x$  away. However, with no symmetry breaking element at play, each step can proceed with equal probability to the right or the left, yielding zero current.

The introduction of a weak probe  $\mathcal{E}_p$ ,  $\omega_p$  propagating in the  $z$ -direction, as in Fig. 1 (a), breaks the symmetry resulting in directed motion along  $\pm x$ :  $\mathcal{E}_p$  modulates the lattice at  $\delta = \omega_L - \omega_p$  producing the following addition to the optical potentials

$$U_{\pm}^p(x) = -2U_0 \varepsilon_p \cos k_x x \cos \delta t, \quad (4)$$

where  $\varepsilon_p = \mathcal{E}_p / 4\mathcal{E}_0$ . Since

$$\cos k_x x \cos \delta t = \frac{1}{2} [\cos(-k_x x - \delta t) + \cos(+k_x x - \delta t)], \quad (5)$$

the probe contribution (4) can be seen as the superposition of two perturbations traveling in opposite directions with velocity  $\pm \delta/k_x$ . Each perturbation is expected to excite an atomic density wave with wave number  $k = \pm k_x$  and frequency  $\omega = \delta$ , referred to as Brillouin modes in analogy to acoustic waves rippling through fluids [19, 20]. Optimal propagation is then expected when the velocity of these atomic modes,  $v_B = \pm \delta/k_x$ , matches that of the half-oscillations discussed above,  $v_S$ , yielding a maximum at  $\delta = \Omega_X$ . Previous research [19–22] has focused only on these modes, which share the same frequency and wave number as the probe perturbations (a rudimentary visualization of such a mode is provided in Sec. S3, supplementary notes). The results of a novel theory [23], presented in Fig. 2, do confirm them as the dominant ones, though other excited density waves can be clearly observed at play with non-negligible quantitative contributions.

In general, a propagating perturbation is expected to excite not only the atomic wave of frequency and wave number of the perturbation, but also other nearby modes. This is indeed the case in our system, Fig. 2 shows that atomic waves with  $\omega = \delta$  and  $k = 2k_x$  and  $3k_x$  are also excited, as well as the mode  $\omega = 2\delta$ ,  $k = 2k_x$ , which has the same phase velocity as the propagating perturbation, in addition to a plethora of non-propagating modes (i.e. with  $\omega = 0$ ).

However, mode excitation is not sufficient to guarantee a significant contribution to the directed motion. In Brownian ratchets [1–3], the quantity of interest is the current, defined as the average velocity  $\langle v \rangle = \lim_{t \rightarrow \infty} [\langle x(t) \rangle - \langle x(0) \rangle] / t$ . A novel theoretical development [23] has been able to express analytically the current as an expansion  $\langle v \rangle = \sum_{l,n} v[l,n]$ , where  $v[l,n]$  is proportional to the Fourier amplitude of the atomic density wave with frequency  $\omega = l\delta$  and wave number  $k = nk_x$ . The analytical calculation is based on the coupled Fokker-Planck equations resulting from the

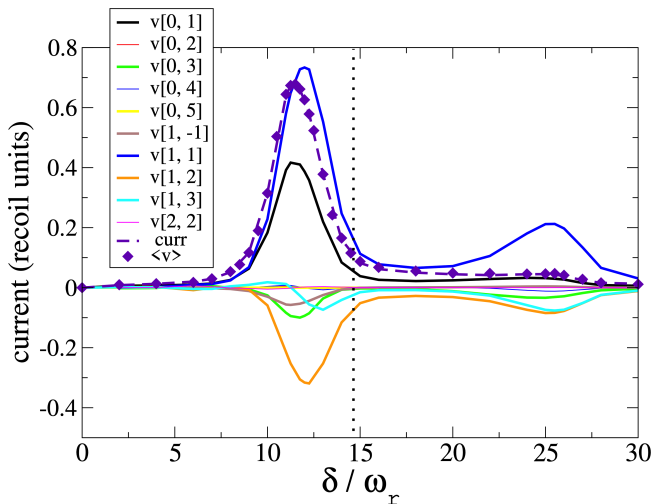


FIG. 2. Contribution to the current  $v[l, n]$  of the atomic density wave with frequency  $\omega = l\delta$  and wave number  $k = nk_x$  under a probe-induced lattice modulation traveling in the  $+x$ -direction (6) with  $\varepsilon_p = 0.1$ , from a semiclassical simulation with  $U_0 = 400 \hbar\omega_r$  and  $\Gamma_S = 5.7 \omega_r$ ,  $\theta_x = 25^\circ$ . The dashed line is the sum of all contributions, and the diamonds the current calculated directly in the simulation. The vertical dotted line indicates the vibrational frequency  $\Omega_X$ .

semiclassical approximation [25]. Fig. 2 shows the results for the optical lattice (1)–(2) modulated by the  $+x$ -propagating part of the probe potential in (4)–(5)

$$U_{\pm}^p(x) = -U_0\varepsilon_p \cos(k_x x - \delta t). \quad (6)$$

The good agreement between the current obtained directly in the simulations (diamonds) and the sum of all the mode contributions (dashed line) serves as a validation of the analytical calculations [23].

As discussed above, optimal transport for atoms following the density mode  $\omega = \delta$ ,  $k = k_x$  is expected when its propagation is synchronized with the most likely transitions between the ground state sublevels, the latter happening at half oscillations in the potential wells, and thus at  $\delta \approx \Omega_X$ . Here an atom could be hopping between states after half oscillations while riding at a maximum of the atomic wave. Indeed, the strongest peak observed in Fig. 2 takes place at a frequency slightly below  $\Omega_X$ . The expression used for the vibrational frequency (3) is based on a harmonic approximation for small deviations about the well's bottoms, actually underestimating the time spent in the half oscillation, and thus, overestimating the optimal frequency.

A second peak, though of considerably smaller amplitude, can be seen at double this optimal frequency in Fig. 2, indicating a further synchronization mechanism between the two propagation processes. It can be also readily rationalized, as in these conditions, during a half oscillation time, the atomic wave, traveling at two times the previous speed, can still offer a density maximum at

the same places where the atomic transitions are most likely, the potential barriers.

Note that Fig. 2 shows important contributions to the directed motion coming from other modes. In particular, the atomic wave with  $\omega = \delta$ ,  $k = 2k_x$  is observed to produce a current, slightly less than half the contribution of the probe's mode, in the opposite direction. In this case the atomic wave is moving with half the speed,  $\delta/(2k_x)$ , and has half the wavelength,  $2\pi/(2k_x)$ , thus there is an extra density maximum within the well length  $2\pi/k_x$ . Under these conditions, an atom moving in the direction of the probe-modulated potential (6) has higher speed than the wave and is less likely to cross a density maximum than when moving in the opposite direction, thus favoring that reversed direction.

Moreover, Fig. 2 shows that the contribution to the current from the mode with  $\omega = 0$ ,  $k = k_x$  is slightly more than half the contribution of the dominant mode, and is therefore relevant. This kind of non-propagating mode is responsible for directed motion in rocking ratchets [1], where the driving force is usually chosen to be unbiased and non-propagating. Here the mode, like all modes shown in Fig. 2, is also observed to be optimally excited at about the vibrational frequency, owing to the discussed matching of  $\delta$  with the intrinsic frequency  $\Omega_X$ .

Note that the transition rates  $\gamma_{\pm}$  define another intrinsic frequency of the unperturbed lattice. Taking the spatial average of (2) results in  $\gamma_0 = 2\Gamma_S/3$ , the average number of atomic transitions per unit time. Thus, a *resonant enhancement* of atoms undergoing directed propagation is expected when  $\gamma_0$  is synchronized with  $\delta$  and  $\Omega_X$ . Specifically, the most coherent motion is expected when there is a single transition every half oscillation,  $\gamma_0(\pi/\Omega_X) \approx 1$ , yielding the prediction [21]

$$\Gamma_S \approx \frac{6}{\pi} \sin \theta_x \sqrt{|\Delta'_0| \omega_r}. \quad (7)$$

Optimization of the unidirectional propagation is therefore expected when the random photon scattering process  $\Gamma_S$  is tuned to the value given by (7). This is stochastic resonance [20–22], which we demonstrate experimentally via pump-probe spectroscopy below.

Our experiments are performed in a standard 3D tetrahedral  $\text{lin} \perp \text{lin}$  lattice, depicted in Fig. 1(a), comprising four equally intense near-resonant red-detuned beams ( $1/e^2$ -diameter, 9.2 mm;  $\theta_x = \theta_y = 25^\circ$ ) that confine about  $10^8$   $^{85}\text{Rb}$  atoms ( $\sim 30 \mu\text{K}$ ), i.e., only a few percent of the wells are occupied by an atom. We introduce a weak  $y$ -polarized  $z$ -propagating probe beam (Z-probe) of intensity  $I_p$  with  $1/e^2$ -diameter 1.4 mm ( $\lesssim$  diameter of cold atom cloud) at frequency  $\omega_p$ . The lattice beams collectively serve as the pump at fixed frequency  $\omega$ . The probe frequency  $\omega_p$  is scanned around  $\omega$ , and probe transmission is measured as a function of the pump-probe detuning  $\delta$ . The intensity for a single lattice beam  $I$  ranges from 1.48 to 14.5 mW/cm<sup>2</sup> (total lattice intensity

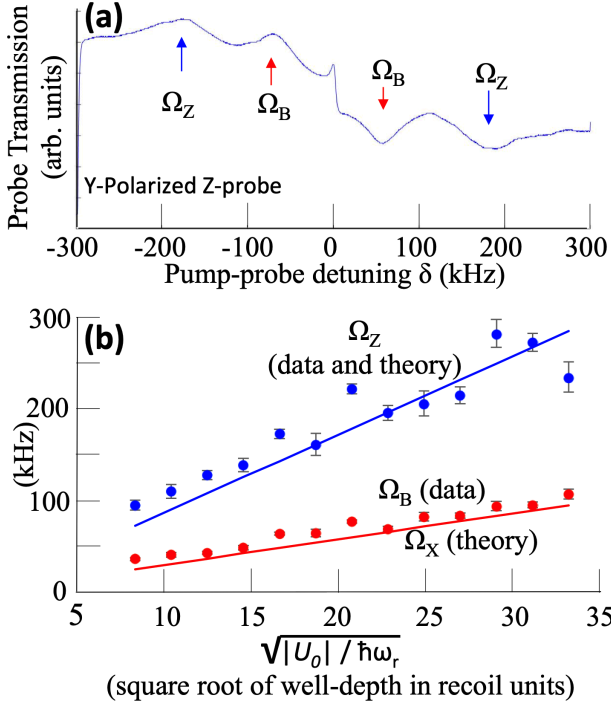


FIG. 3. (a) Typical probe transmission spectrum for the 3D tetrahedral lin||lin lattice with weak  $y$ -polarized  $z$ -propagating probe, at well-depth  $|U_0|/\hbar = 276 \omega_r$  ( $I = 5.2$  mW/cm<sup>2</sup>,  $\Delta = -12\Gamma$ ; 10 ms for each scan). We observe a feature  $\Omega_Z$  at  $\sim \pm 170$  kHz, and additional resonances  $\Omega_B$  at  $\sim \pm 60$  kHz which arise from probe-induced directed atomic transport along  $\pm x$ . (b) Measured values for  $\Omega_Z$  and  $\Omega_B$  versus well-depth agree with calculations (lines) of the  $z$ -component of the vibrational frequency and  $x$ -component  $\Omega_X$ , respectively (see text). Here,  $\omega_r$  is the <sup>85</sup>Rb recoil frequency 3.86 kHz. No fitting parameters are used.

$= 4I$ ), and the lattice is red-detuned by  $\Delta = 3.5 - 17 \Gamma$  from the <sup>85</sup>Rb  $F_g = 3 \rightarrow F_e = 4 D_2$  transition (natural linewidth  $\Gamma/2\pi = 6.07$  MHz). In all cases  $\delta/\omega < 10^{-9}$  and the intensity ratio of probe-to-single lattice beam is  $|\mathcal{E}_p/\mathcal{E}_0|^2 < 4\%$ , i.e.,  $I_p/4I < 1\%$ .

To explore stochastic resonance we tune the random noise  $\Gamma_S$  without changing the optical lattice, described by well depth  $U_0$ . From (S1-S6), supplementary notes we see that if we tune lattice intensity  $I$  and detuning  $\Delta$  such that the ratio  $I/\Delta$  remains constant, we may vary  $\Gamma_S$  ( $\propto I/\Delta^2$ ) without changing  $U_0$  ( $\propto I/\Delta$ ).

Fig. 3(a) shows the probe transmission spectrum for a specific lattice well-depth. A spectral feature denoted  $\Omega_Z$  arises because the  $Z$ -probe induces Raman transitions between adjacent vibrational levels in each well [19], in this case separated by  $\sim \pm 170$  KHz. The peak (dip) corresponds to photons absorbed from a pump beam (the probe) and emitted into the probe (a pump beam). Further, we observe Brillouin resonances denoted as  $\Omega_B$  which are a signature of directional transport as explained below. Fig. 3(b) shows that the observed  $\Omega_Z$  and  $\Omega_B$ -values, as the well-depth is varied, are in good agreement with the calculated values, shown by lines, for

$\Omega_Z$  ((S5), supplementary notes) and  $\Omega_X$  (3), respectively.

The features  $\Omega_B$ , despite coinciding with  $\pm\Omega_X$ , cannot arise from non-propagating atoms oscillating inside wells, because the  $Z$ -probe operator is quadratic in  $x$  (Sec. S4, supplementary notes). Instead, the  $Z$ -probe interferes with the lattice beams, producing propagating modulations that drive directed transport. Note that the contributions to the pump-probe spectrum from two of the four lattice beams,  $\vec{k}_3$  and  $\vec{k}_4$ , are suppressed due to Doppler-broadening in the  $z$ -direction [26].

The interference of the  $\hat{y}$ -polarized probe with  $\hat{y}$ -polarized lattice beams  $\vec{k}_1, \vec{k}_2$  ( $|\vec{k}_{1,2}| = |\vec{k}_p| = k$ ) generates a propagating *intensity* modulation in directions  $\pm x$  (4-5). As discussed above, optimal directed propagation is expected at  $\delta = \pm\Omega_X$ , precisely the features marked  $\Omega_B$  in Fig. 3(a). This velocity class, instead of diffusing in all directions, is ratcheted along  $\pm x$ , yielding a bidirectional ratchet.

In a significant departure from previous works, we shift attention from the location of the peak  $\Omega_B$  to the *peak-amplitude*  $\mathcal{A}$  which is proportional to the *number of atoms ratcheted* along  $\pm x$ . Figs. 4 and 5 show measurements of  $\mathcal{A}$  in the probe-modulated 3D lattice as a function of the stochastic noise rate  $\Gamma_S$ . Each data point is an average  $\mathcal{A}$ -value measured from at least five scans similar to Fig. 3 (a) (see inset, Fig. 4), using a curve-fitting procedure (Sec. S5, supplementary notes). If the number of atoms initially confined in the lattice is kept the same (within 7% in our case), and  $I/\Delta$  is held constant as we vary  $\Gamma_S$ , the  $\mathcal{A}$ -values are a measure of the directed atomic current for different noise rates.

Fig. 4 shows clear evidence for stochastic resonance in a modulated cold atom optical lattice for three probe modulation strengths  $I_p/4I$  ranging from 0.25% to 0.85%. Increasing the modulation strength results in larger atomic current, but since the lattice, and therefore vibrational

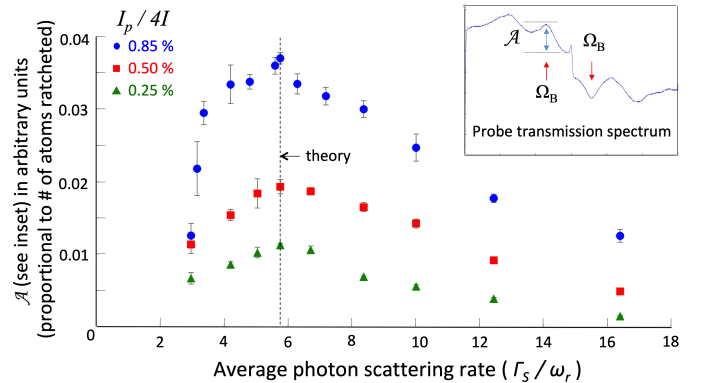


FIG. 4. Number of atoms ratcheted along  $\pm x$  versus noise rate, or more specifically: Amplitude of Brillouin peak  $\Omega_B$  vs.  $\Gamma_S$  the photon scattering rate per lattice beam in units of recoil frequency  $\omega_r$ , at a fixed well-depth ( $|U_0|/\hbar \approx 400\omega_r$ ). Stochastic resonance is observed at  $\Gamma_S/\omega_r = 5.7$  irrespective of modulation amplitude, in agreement with theory (7).

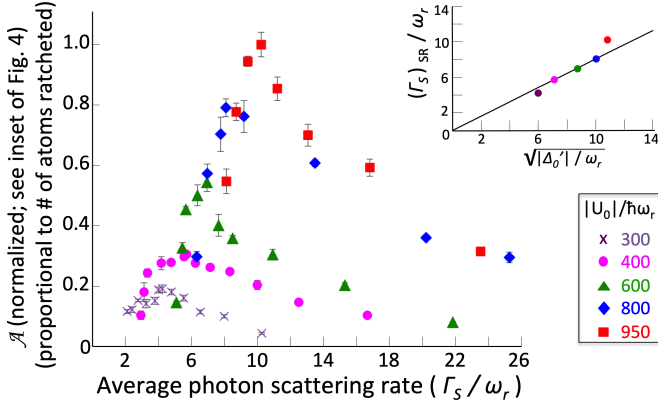


FIG. 5. Number of atoms ratcheted along  $\pm x$  vs. noise rate, for different well-depths  $|U_0|/\hbar\omega_r$  at fixed modulation strength  $I_p/4I = 0.85\%$ . Inset: The noise rate  $(\Gamma_S)_{SR}$  at which stochastic resonance occurs scales linearly with  $\sqrt{|\Delta'_0|}$  in agreement with theory (7).

frequency, remains unchanged we observe stochastic resonance at the same  $\Gamma_S$ -value. Atomic transport in this bidirectional ratchet falls off on either side of stochastic resonance, faster for low  $\Gamma_S$ -values since well-to-well transfer is disrupted more effectively if optical pumping simply does not occur. These observations concur with numerical simulations in Ref. [21] of the diffusion coefficient predicting enhanced transport along  $\pm x$ .

Furthermore, the noise rate at which stochastic resonance occurs is seen in Fig. 4 to be in very good agreement with the prediction of (7). This agreement is remarkable considering that the prediction in (7) uses a  $F_g = 1/2 \rightarrow F_e = 3/2$  atom. In Fig. 5 we test the theory further by fixing the modulation strength and investigating stochastic resonance for several different well-depths. In the inset we denote the noise rate at which stochastic resonance occurs as  $(\Gamma_S)_{SR}$ , and experimentally verify the linear dependence of  $(\Gamma_S)_{SR}$  on the square root of the light shift  $\Delta'_0$ . The requirement to keep the modulation strength fixed while varying well-depth ( $\propto I$ ) means that at the highest well-depth the probe intensity is strong enough to perturb the lattice, while at the lowest well-depth  $I_p$  is weak and barely excites Brillouin propagation, causing the data to depart from theory in both cases.

In conclusion, we have unambiguously demonstrated stochastic resonance in a dissipative optical lattice. By observing the transmission spectrum of a weak probe beam that modulates the lattice we present evidence that the photon scattering rate at which stochastic resonance occurs is independent of the modulation strength, and that the stochastic resonance can be controlled by varying the lattice well depth. Remarkably, the data agrees well with theory based on a simple  $F_g = 1/2 \rightarrow F_e = 3/2$  atom without use of any fitting parameters. Furthermore, a recent novel theory has permitted us to precisely determine the contribution to the directed motion of the atomic density waves excited by the perturbing probe, and how they conspire with the optical pumping rates

to create resonant directional propagation within a randomly diffusing cold atom cloud.

\* Corresponding author: balis@miamioh.edu

† These two authors contributed equally.

- [1] D. Cubero and R. Renzoni, *Brownian Ratchets: From Statistical Physics to Bio and Nano-motors* (Cambridge University Press, 2016)
- [2] P. Hänggi, F. Marchesoni, Rev. Mod. Phys. **81**, 387 (2009)
- [3] P. Reimann, Phys. Rep. **361**, 57 (2002)
- [4] T. Wellens, V. Shatokhin, and A. Buchleitner, Rep. Prog. Phys. **67**, 45 (2004)
- [5] L. Gammaitoni, P. Hänggi, P. Jung, and F. Marchesoni, Rev. Mod. Phys. **70** (1), 223 (1998)
- [6] K. Wiesenfeld and F. Moss, Nature **373**, 33 (1995)
- [7] A. Ganapolski and S. Rahmstorf, Phys. Rev. Lett. **88**, 038501 (2002)
- [8] M. McDonnell and D. Abbott, PLoS Comp. Bio. **5**(5): e1000348 (2009)
- [9] B. Bhar, et al., Sci. Rep. **10**, 5549 (2020)
- [10] A. Dodda, et al., Nat. Comm. **11**, 4406 (2020)
- [11] B. Lewandowski *et al.*, Science **339**, 189 - 193 (2013)
- [12] T. Wagner, P. Talkner, J. Bayer, E. Rugeramigabo, P. Hänggi, and R. Haug, Nat. Phys. **15**, 330 - 334 (2019)
- [13] S. Ludwig, Nat. Phys. **15**, 310 - 311 (2019)
- [14] J. P. Pekola, Nat. Phys. **11**, 118 (2015)
- [15] D. Mason, et al., Nat. Phys. **15**, 745 (2019)
- [16] A. Heinrich, et al., Nat. Nanotechnol. **16**, 1318 (2021)
- [17] G. Grynberg, C. Robilliard, Phys. Rep. **355**, 335 (2001)
- [18] I. Stroescu, D. Hume, and M. Oberthaler, Phys. Rev. Lett. **117**, 243005 (2016)
- [19] J.-Y. Courtois, S. Guibal, D. Meacher, P. Verkerk, and G. Grynberg, Phys. Rev. Lett. **77**, 40 (1996)
- [20] L. Sanchez-Palencia, F. Carminati, M. Schiavoni, F. Renzoni, and G. Grynberg, Phys. Rev. Lett. **88**, 133903 (2002)
- [21] L. Sanchez-Palencia and G. Grynberg, Phys. Rev. A **68**, 023404 (2003)
- [22] M. Schiavoni, F. Carminati, L. Sanchez-Palencia, F. Renzoni and G. Grynberg, Europhys. Lett. **59** (4), 493 (2002)
- [23] D. Cubero, arXiv:2208.08206 (2022)
- [24] P. Horak, J.-Y. Courtois, and G. Grynberg, Phys. Rev. A **58**, 3953 (1998)
- [25] K. Petsas, G. Grynberg, and J.-Y. Courtois, Eur. Phys. J. D **6**, 29 (1999)
- [26] C. Jurczak, J.-Y. Courtois, B. Desruelle, C.I. Westbrook, and A. Aspect, Eur. Phys. J. D **1**, 53 (1998)

## ACKNOWLEDGEMENTS

This work is supported by the Army Research Office under award/contract number W911NF2110120. DC acknowledges financial support from the Ministerio de Ciencia e Innovación of Spain of Spain, Grant No. PID2019-105316GB-I00. We gratefully acknowledge electronics and LabView support by the Instrumentation Laboratory at Miami University. We thank A. Dharasiri and A. Rapp for assistance during the initial setup. We are grateful to A. Reinhard and N. Peters for providing invaluable feedback on the manuscript.



## Supplementary material: Observation of stochastic resonance in directed propagation of cold atoms

A.Staron<sup>1,†</sup>, K. Jiang<sup>1,†</sup>, C. Scoggins<sup>1</sup>, D. Wingert<sup>1</sup>, D. Cubero<sup>2</sup>, and S. Bali<sup>1</sup>

<sup>1</sup> *Department of Physics, Miami University, Oxford, Ohio 45056-1866, USA*

<sup>2</sup> *Departamento de Fisica Aplicada I, Universidad de Sevilla, Spain*

<sup>†</sup> *These two authors contributed equally*

Here, we provide additional proofs and justifications for statements made in the main text. Sections S1 and S2 summarize relevant background on dissipative optical lattices: Section S1 starts with the conceptually simpler one-dimensional configuration, while Section S2 focuses on the three-dimensional setup used in the reported experiments. In Section S3 we provide a rudimentary visualization of the dominant [1,1] Brillouin mode that propagates at the same frequency and wave number as the probe perturbation. Section S4 discusses the association of  $\Omega_B$  in Fig. 3 with a propagating mode. In Section S5 we describe the fit function used to model our measured probe transmission spectra.

### S1 1D dissipative optical lattice

Dissipative optical lattices are an ideal testbed for studying stochastic resonance because the stochastic coupling between the system (confined atom) and environment (random fluctuations in energy in the form of photon scattering) can be precisely controlled by varying the laser intensity and detuning, while ensuring that the lattice well-depth remains constant. This essential point can be conveyed using a 1D lin $\perp$ lin lattice and a  $F_g = 1/2 \rightarrow F_e = 3/2$  atom where  $F$  is the hyperfine quantum number.

Two counterpropagating red-detuned laser beams  $\vec{E}_1$  and  $\vec{E}_2$  of orthogonal linear polarization but same amplitude and wavelength  $\lambda$  are superposed as in Fig. S1(a), yielding constant intensity but with steep polarization gradient of pitch  $\lambda/2$ .

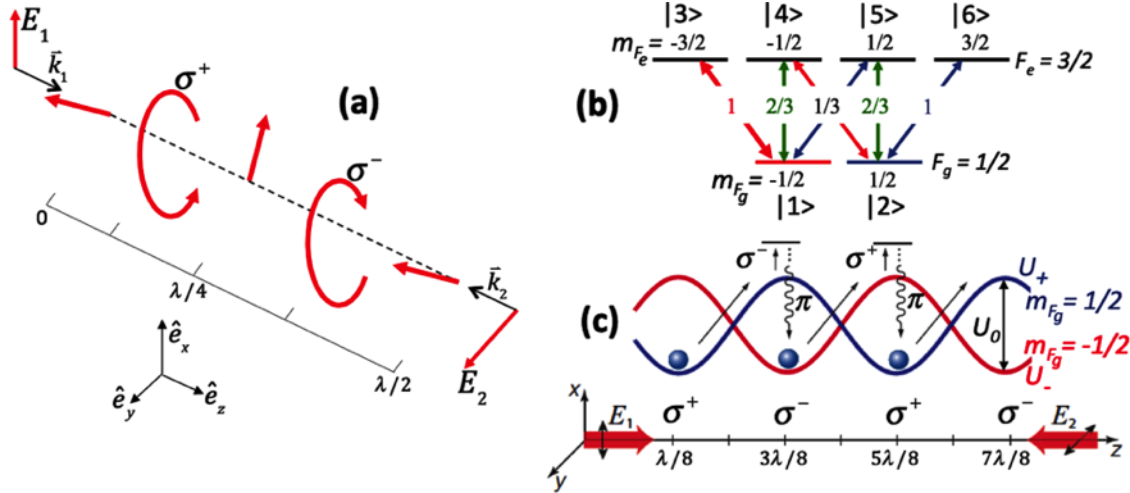


Figure S1: (a) Polarization gradient in 1D lin  $\perp$  lin  $\vec{E}$ -field configuration, and (b) Clebsch-Gordon coefficients for  $F_g = 1/2 \rightarrow F_e = 3/2$  atom, lead to (c) bi-potential  $U_{\pm}$  with well-depth  $U_0$ .

Fig. S1(b) shows the Clebsch-Gordan coefficients and our numbering scheme  $|1\rangle - |6\rangle$  for the six Zeeman energy-levels. The two ground state magnetic sub-levels  $m_{F_g} = \pm 1/2$  undergo polarization-dependent AC Stark shifts yielding spatially modulated potential wells  $U_{\pm}(z)$  which have maximum

depth  $U_1$  at sites of alternating pure circular polarization, shown in Fig. S1(c). Each atom is Sisyphus-cooled, eventually settling in a well where it oscillates with frequency  $\Omega_V$ . The oscillatory excursions away from sites of pure circular polarization cause optical pumping to an adjacent well on either side, leading to diffusion along  $\pm z$ .

In the weak excitation limit, the light-shifted bi-potential  $U_{\pm}(z)$  and 1D lattice well-depth  $U_0$ , along with the intra-well vibrational frequency  $\Omega_V$ , are given by the well-known expressions below for a  $F_g = 1/2 \rightarrow F_e = 3/2$  atom. Also, the position-dependent transition probability rates between the ground state potentials  $\gamma_{\pm}$  are expressed below [1, 2, 3, 4]:

$$U_{\pm}(z) = \frac{U_0}{2} [-2 \pm \cos 2k_L z], \text{ where}$$

$$U_0 = \text{1D lattice well-depth in Fig. S1(c)} = -\frac{4}{3}\hbar\Delta_0' = -\frac{2}{3} \left( \frac{I/I_{sat}}{1 + 4\Delta^2/\Gamma^2} \right) \hbar\Delta \propto \frac{I}{|\Delta|} \quad (\text{S1})$$

$$\Omega_V = 2\sqrt{\omega_r U_0/\hbar} \propto \sqrt{\frac{I}{|\Delta|}} \quad (\text{S2})$$

$$\gamma_{\pm}(z) = \frac{2\Gamma_S}{9} (1 \pm \cos 2k_L z), \text{ where } \Gamma_S = \frac{\Gamma}{2} \left( \frac{I/I_{sat}}{1 + 4\Delta^2/\Gamma^2} \right) \propto \frac{I}{\Delta^2} \quad (\text{S3})$$

Here  $I$  is the lattice laser intensity (per beam) and  $I_{sat}$  is the saturation intensity,  $\Delta$  is the lattice laser detuning ( $< 0$ ),  $\Gamma/2\pi$  is the natural linewidth and  $\omega_r/2\pi$  is the recoil frequency (6.07 MHz and 3.86 kHz, respectively, for  $^{85}\text{Rb}$ ),  $k_L = 2\pi/\lambda$ , and  $z$  is the lattice axis. The relation  $|\Delta| \gg \Gamma$  usually applies in practical situations. The ratio  $(I/I_{sat})/(1 + 4\Delta^2/\Gamma^2)$  is just the saturation parameter  $s_0$  which is  $\ll 1$  in the weak excitation limit. In our 3D lattice experiments  $s_0$  ranges from about 0.001 to about 0.08.  $\Delta_0' \equiv \Delta s_0/2$  is the light-shift per lattice beam for a closed transition having a Clebsch - Gordan coefficient equal to 1, in accordance with notation used in Refs. [1] and [4]. Similarly,  $\Gamma_S \equiv \Gamma s_0/2$  is the photon scattering rate per lattice beam [4].

From Eqns. S1 - S3 we see that if we tune  $I$  and  $\Delta$  such that  $I/\Delta^2$  varies but  $I/|\Delta|$  stays constant, we can tune the stochastic noise given by the photon scattering rate  $\Gamma_S$  while keeping the lattice unchanged (because the well-depth  $U_0$  and vibrational frequency  $\Omega_V$  stay constant). This ability to tune the stochastic noise while leaving the lattice unchanged makes the dissipative lattice a uniquely ideal testbed for investigating stochastic resonance.

## S2 3D dissipative tetrahedral optical lattice

Our experiments on stochastic resonance are carried out in a three-dimensional standard lin⊥lin dissipative “bright” optical lattice. A standard 3D tetrahedral lin⊥lin lattice consists of four overlapping equally intense near-resonant red-detuned beams as shown in Fig. S2 (same as Fig. 1a in the main paper, but without the probe beam). The total electric field now takes the form [1]:

$$\vec{E}(z, t) = \frac{1}{2} \mathcal{E}_0 \left( e^{i\phi} \hat{e}_y e^{i\vec{k}_1 \cdot \vec{r}} + e^{i\phi} \hat{e}_y e^{i\vec{k}_2 \cdot \vec{r}} + \hat{e}_x e^{i\vec{k}_3 \cdot \vec{r}} + \hat{e}_x e^{i\vec{k}_4 \cdot \vec{r}} \right) e^{-i\omega_L t} + c.c.$$

$$\text{where } \vec{k}_1 \cdot \vec{r} = k_L(x \sin \theta_x + z \cos \theta_x), \quad \vec{k}_2 \cdot \vec{r} = k_L(-x \sin \theta_x + z \cos \theta_x)$$

$$\vec{k}_3 \cdot \vec{r} = k_L(x \sin \theta_y - z \cos \theta_y), \quad \vec{k}_4 \cdot \vec{r} = k_L(-x \sin \theta_y - z \cos \theta_y)$$

where the choice  $e^{i\phi} = -i$  is made as in Ref. [1].

For a  $F_g = 1/2 \rightarrow F_e = 3/2$  atom confined in this 3D lattice the equations corresponding to Eqns. S1 - S3 are derived in Refs. [1, 3, 4]:

$$U_{\pm}(x, y, z) = \frac{U_0}{4} [-2 - \cos(2k_x x) - \cos(2k_y y) \pm 2\cos(k_x x) \cos(k_y y) \cos(k_z z)], \text{ where} \\ U_0 = 3\text{D lattice well-depth in Fig. 1(b)} = -16\hbar\Delta'_0/3 \quad (\text{S4})$$

$$\Omega_{X,Y} = 4 \sin \theta_{x,y} \sqrt{|\Delta'_0| \omega_r}, \quad \Omega_Z = (\cos \theta_x + \cos \theta_y) \sqrt{|\Delta'_0| \omega_r} \quad (\text{S5})$$

$$\gamma_{\pm}(x, y, z) = \frac{2\Gamma_S}{9} [2 + \cos(2k_x x) + \cos(2k_y y) \pm 4 \cos(k_x x) \cos(k_y y) \cos(k_z z)] \quad (\text{S6})$$

where  $k_x = k_L \sin \theta_x$ ,  $k_y = k_L \sin \theta_y$ , and  $k_z = k_L(\cos \theta_x + \cos \theta_y)$ .  $\Omega_{X,Y,Z}$  are the  $x, y, z$ -components of the vibrational frequency  $\Omega_V$ . Note that the expression for  $\Omega_Z$  above is modified so as to be a better approximation for the case of a  $F_g \geq 3 \rightarrow F_e = F_g + 1$  atom [1].  $\Delta' = 8\Delta'_0$  is the light-shift at a point of circular polarization for a closed transition having a Clebsch - Gordan coefficient equal to 1. For the  $F_g = 3 \rightarrow F_e = 4$  transition in  $^{85}\text{Rb}$ ,  $I_{sat} = 1.64 \text{ mW/cm}^2$  for  $\sigma$ -light.

In the experiments, a  $y$ -polarized probe beam of the form [1]

$$\vec{E}_p(z, t) = e^{i\phi} \hat{e}_y \mathcal{E}_p e^{i(k_p z - \omega_p t)} + c.c. \quad (\text{S7})$$

propagating in the  $+z$ -direction is made incident on the 3D lattice, as depicted in Fig. 1(a).

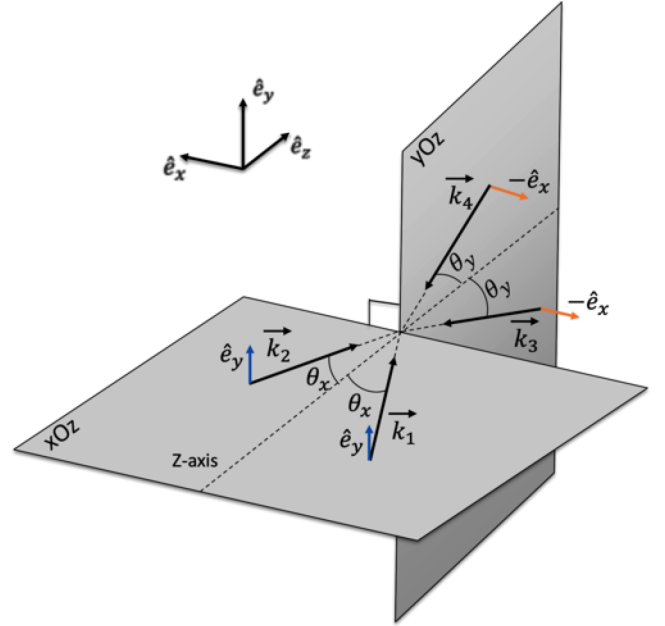


Figure S2: 3D tetrahedral lin⊥lin lattice configuration. Beams  $\vec{k}_1, \vec{k}_2$  ( $\vec{k}_3, \vec{k}_4$ ) propagate in the  $x$ - $z$  ( $y$ - $z$ ) plane with polarization along the  $\hat{y}$  ( $\hat{x}$ ) direction.



### S3 Probe-modulated 1D dissipative optical lattice: A rudimentary visualization of the dominant mode [1,1] in Fig. 2 of main paper

In the main paper, the results of a new theory [5] for Brillouin propagation in a 1D section of a 3D lattice are summarized. The atomic current is decomposed into the contributions from the different atomic density wave modes that are excited by the weak probe. The  $z$ -propagating probe creates a lattice perturbation that propagates in the  $\pm x$ -directions, and the dominant mode is shown to be the atomic density wave that propagates at the same velocity as the propagating potential perturbation.

While previous theoretical treatments of Brillouin propagation [4, 6, 7, 8] lack rigor in the sense that they focus only on the dominant [1,1] mode (see Fig. 2 in the main paper) and ignore the contributions from other modes that are excited by the probe, they do offer some instructive insights into how directed atomic propagation may arise within a sample of randomly diffusing atoms. One may proceed by considering a simple model of a fictitious  $F_g = 1/2 \rightarrow F_e = 3/2$  atom confined in a 1D lin $\perp$ lin optical lattice with wells  $\lambda/4$  apart as shown in Fig. S1(c). Atoms oscillate in the wells of this 1D lattice with vibrational frequency  $\Omega_V$ , given by (S2). As mentioned in the main paper, since the atoms are most likely pumped to a neighboring well via sublevel transitions at the turning points in their oscillations, i.e., after half a time-period  $\pi/\Omega_V$ , the average speed associated with this half-oscillation is given by  $v_S = \Omega_V/(2k_L)$ . The pumping is equally likely to occur in the  $\pm z$ -directions yielding zero current.

However, when the lattice is illuminated by a weak probe beam which is polarized parallel to the counter-propagating laser beam, as shown in Fig. S3, the symmetry is broken which results in a net current as we shall see below.

The probe frequency  $\omega_p$  is scanned around the lattice beam frequency  $\omega$  by a small amount  $\delta$ . The interference between the similarly polarized probe and the counter-propagating lattice beam yields a propagating intensity modulation moving with velocity  $\delta/(2k_L)$ , where  $2\pi/k_L$  equals the laser wavelength  $\lambda$ . The probe and co-propagating lattice beam do not yield a propagating modulation so that interaction is ignored.

The optical bipotential  $U_{\pm}(z)$  for the ground states depicted in Fig. S1(c) is modulated by the probe and becomes [9]:

$$U_{\pm} = \frac{U_0}{2} \left[ (-2 \pm \cos 2k_L z) + \frac{\mathcal{E}_p}{\mathcal{E}_0} [-2 \cos(2k_L z - \delta t) \pm \cos \delta t] \right]. \quad (\text{S8})$$

The intensity modulation also affects the optical pumping rates between ground states. We may simply track these effects by calculating the probe-induced modifications to the steady-state ground-level populations  $\rho_{\pm}$  [10], denoted by  $\Delta\rho_{\pm} \equiv \rho_{\pm, \text{probe}} - \rho_{\pm, \text{no probe}}$ .

Here,  $\rho_{\pm, \text{no probe}} = \frac{\cos^2 k_L z}{\sin^2 k_L z}$  as is well known [1], and for a closed system,  $\Delta\rho_+ + \Delta\rho_- = 0$ . We find:

$$\Delta\rho_{\pm}(z, t) = \mp \frac{\mathcal{E}_p}{2\mathcal{E}_0} \frac{\sin 2k_L z \sin(2k_L z - \delta t)}{1 + \frac{\mathcal{E}_p}{\mathcal{E}_0} \cos(2k_L z - \delta t)} \quad (\text{S9})$$

A positive (negative) value for, say,  $\Delta\rho_+(z, t)$  tells us that the tendency for atoms to be optically pumped by the probe from  $U_-$  into  $U_+$  (from  $U_+$  into  $U_-$ ) is enhanced at that particular point in space and time.

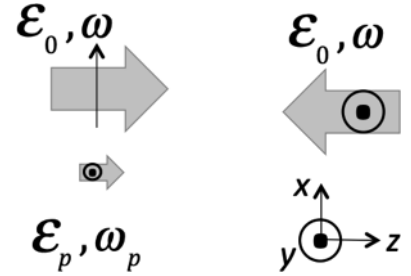


Figure S3: Geometry for 1D lin $\perp$ lin lattice illuminated by a weak probe  $\vec{\mathcal{E}}_p$  polarized parallel to the counter-propagating lattice beam, yielding a propagating intensity modulation.

In Fig. S4 (A - I) we plot successive snapshots at  $\delta t = 0, \pi/4, \pi/2$ , and so on, of  $U_{\pm}$  and  $\Delta\rho_{\pm}$  using Eqns. S8 and S9, and depict an atom moving on  $U_{\pm}$  with velocity  $+v_S$ . We use  $\epsilon_p = \mathcal{E}_p/2\mathcal{E}_0 = 0.1$ , same as in Eqn. (4) of the main paper. In the top plot the probe is OFF:  $\Delta\rho_{\pm} = 0$ , and  $U_{\pm}$  depict the original ground state bipotential. The gray region marks the size of the original (unmodified) well-depth, and the dashed vertical lines mark the original well-locations before the probe is turned on. When the probe is turned ON, the potentials  $U_{\pm}(z, t)$  are modulated out-of-phase with each other, as they shift in location side-to-side (shown by the dashed vertical arrows on the left side of the figure) and also vary in depth. Spatial symmetry is broken yielding directional motion because the bipotential is modulated asymmetrically. For concreteness, consider an atom starting at  $t = 0$  located on the left side of a  $U_-$ -well near a  $U_+$  crossing point, and moving with mean velocity  $+v_S$ , as depicted in Fig. S4 (A). The figure shows that the atom experiences a deeper well when  $U_-$  shifts rightward (A  $\rightarrow$  B  $\rightarrow$  C) during the  $\delta t = 0 \rightarrow \pi/2$  leg, and a shallower well when  $U_-$  shifts back (C  $\rightarrow$  D  $\rightarrow$  E) during the  $\delta t = \pi/2 \rightarrow \pi$  leg, yielding a net rightward force over the  $\delta t = 0 \rightarrow \pi$  part of the modulation cycle, which serves to collect the atoms on to the right side of the wells near the crossing points. In Fig. S4 the white arrows depict the size and direction of the force at each instant on the atom (not the direction of motion of the atom; the atom is always moving to the right).

Further, note that in Fig. S4 (E), as the atom in  $U_-$  approaches the crossing point with  $U_+$ ,  $\Delta\rho_-$  decreases and  $\Delta\rho_+$  increases, meaning the tendency to be optically pumped into  $U_+$  is enhanced by the probe. The likelihood for transfer is strongest at the crossing point where  $\Delta\rho_+ - \Delta\rho_-$  is maximum, indicated by the vertical black arrow. Fig. S4I shows a similar situation with  $+/-$  notation interchanged.

Thus atoms such as the one depicted in Fig. S4, collect on to the right side of the wells near the  $U_{\pm}$ -crossing points, from where they are optically pumped to the adjacent well, forming a density wave propagating at velocity  $+v_S$ .

As noted above, these atoms complete a half-oscillation in a well between adjacent crossing points in time  $\pi/\Omega_V$ . We see from Fig. S4 that this is the same time as a half-modulation cycle  $\pi/\delta$ , thus yielding the frequency condition:  $\delta = \Omega_V$ , analogous to the  $\delta = \Omega_X$  condition deduced for the 3D lattice in the main paper.

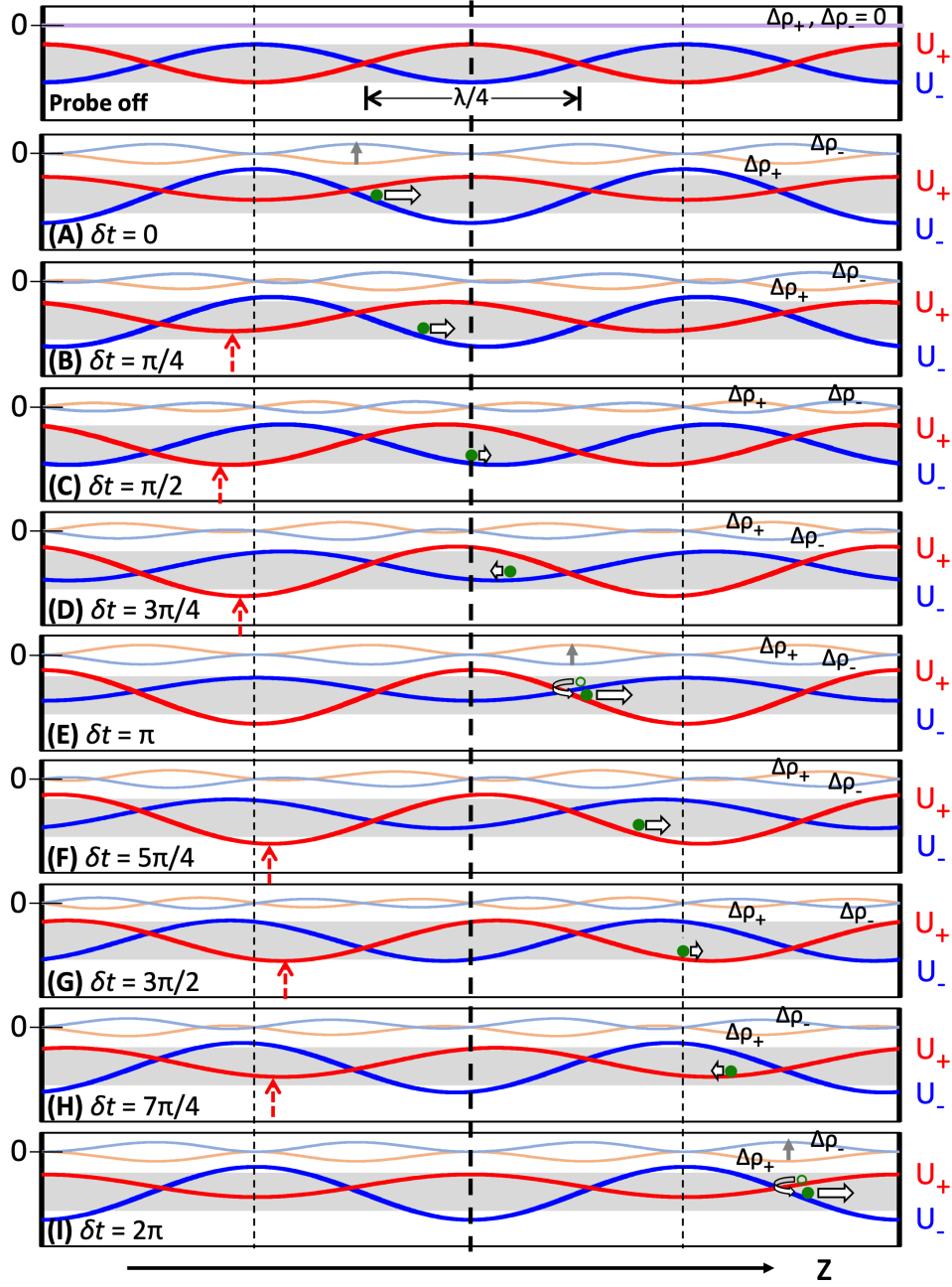


Figure S4: Probe-modified 1D lattice potentials  $U_{\pm}$  (bold curves; (S8)) and probe-induced changes in ground steady-state populations  $\Delta\rho_{\pm}$  (light curves; (S9)). **(Top)** Probe OFF:  $\Delta\rho_{\pm} = 0$ . The location of the unmodified lattice bipotential, depicted by  $U_{\pm}$ , is marked in this plot and all subsequent plots by the gray region and the dashed vertical lines. **(A - I)** Probe ON: Snapshots of  $U_{+}$  and  $U_{-}$  as they are modulated out-of-phase with each other - they shift side-to-side (shown for one of the  $U_{+}$  wells by dashed vertical arrows), and vary in depth. The white arrows depict the instantaneous force sensed by an atom that is continually moving to the right with velocity  $v_S$ . The wells are deeper when they shift rightward, and shallower when they shift left, causing atoms to accumulate on the right side of the wells near the crossing points from where they are highly likely to be pumped to the adjacent well (i.e.,  $|\Delta\rho_{+} - \Delta\rho_{-}|$  maximizes at those locations, as indicated by the vertical gray solid arrow in figs. (E) and (I)). Thus the spatial symmetry is broken by the probe, and a density wave propagating in the  $+z$ -direction is set up. See text for further explanation.

#### S4 $\Omega_B$ in Fig. 3 coincides with $\pm\Omega_X$ but is evidence for directed propagation

In the main paper, experimental evidence for directed propagation, in the form of a bidirectional ratchet along  $\pm x$  (in a 3D dissipative lattice configuration as in Fig. 1(a)), is manifested in Fig. 3(a) as resonances  $\Omega_B$  in the probe transmission spectrum.

The  $z$ -propagating probe is expected to measure  $\Omega_Z$ , but it cannot measure the  $x$ - or  $y$ -components of the vibrational frequency ( $\Omega_X$  or  $\Omega_Y$ ). It is important to make this distinction because  $\Omega_B$  happens to coincide with the calculated value for  $\Omega_X$ . Fig. 3(a) in the paper shows a Z-probe transmission spectrum for a specific lattice well-depth. In order for a peak or a dip at a vibrational frequency component to arise in the probe transmission spectrum there must be a probe-induced Raman transition between adjacent intrawell quantized vibrational levels (say  $\phi_n$  and  $\phi_{n+1}$ , which have opposite parity). Since the probe  $\vec{E}_p$  is weak, the dominant probe term in the total electric field is the lattice-probe interference term which goes as  $\vec{E}_0 \cdot \vec{E}_p^*$  (see Sec. S2). The Raman transition is proportional to the overlap integral  $\int d\vec{r} \phi_{n+1}^* \vec{E}_0 \cdot \vec{E}_p^* \phi_n$ . The product of the wavefunctions is always odd, therefore this integral is nonzero only if the interference term is odd. For the  $y$ -polarized Z-probe, the interference term goes as  $\cos(kx \sin \theta_x) \exp[-ikz(1 - \cos \theta_x)]$ , which for small values of  $x$  and  $z$  is linear in  $z$ , but quadratic in  $x$  (we have taken  $k_L = k_p = k$ ). Thus, the integrand of the overlap integral is even in  $z$  allowing for the detection of Raman transitions at  $\Omega_Z$  in Fig. 3(a). However, the observed peak-dip features at  $\Omega_X$  in Fig. 3(a) cannot arise from Raman transitions between adjacent vibrational levels because the integrand is an odd function in  $x$ . We explain in the main paper that these spectral features actually arise from directional propagating modes along  $\pm x$ .

#### S5 Curve-fitting procedure to obtain $\mathcal{A}$

A typical probe transmission spectrum as in Fig. 3(b) is fit by a function  $I(\delta)$  using the equation

$$\begin{aligned}
 I(\delta) = & A_{Z1} e^{-\frac{(\delta - \Omega_{Z1})^2}{2\sigma_{Z1}^2}} + A_{Z2} e^{-\frac{(\delta - \Omega_{Z2})^2}{2\sigma_{Z2}^2}} \\
 & + A_{B1} e^{-\frac{(\delta - \Omega_{B1})^2}{2\sigma_{B1}^2}} + A_{B2} e^{-\frac{(\delta - \Omega_{B2})^2}{2\sigma_{B2}^2}} \\
 & + a_1 + a_2 \delta + \frac{a_3}{(\delta + x_0)^2 + \gamma^2} \\
 & + \frac{a_4(\delta + x_0)}{(\delta + x_0)^2 + \gamma^2}
 \end{aligned}
 \tag{S10}$$

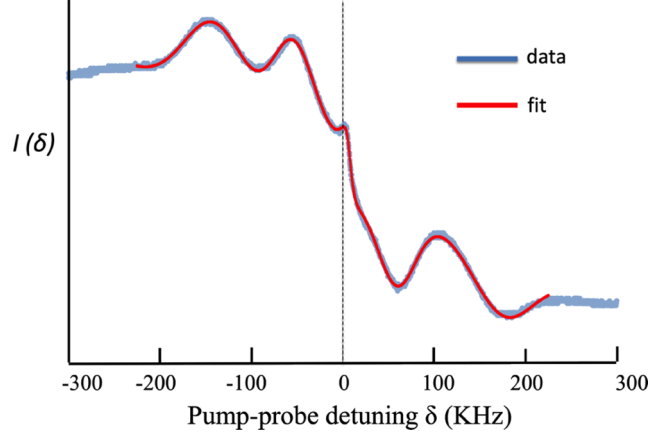


Figure S5: The fit function  $I(\delta)$  defined in Eqn. S10 is used to model the probe transmission spectrum.

The fit function  $I(\delta)$  contains four Gaussian functions, two for the spectral peak and dip at the  $z$ -component of the vibrational frequency  $\pm\Omega_Z$  and two for the Brillouin peak/dip at  $\pm\Omega_B$ .  $I(\delta)$  also contains a combination of Lorentzian and dispersive curves to help fit the central feature of the spectrum - this has been referred to as the “Rayleigh” feature in the literature [1], and is believed to arise from atomic velocity damping due to Sisyphus cooling in the optical lattice [11]. Finally, a linear and constant term are included to further improve the fitting. As shown in Fig. S4,  $I(\delta)$  fits the experimental data well.

# Bibliography

- [1] G. Grynberg and C. Robilliard, *Phy. Rep.* **355**, 335 - 451 (2001)
- [2] J. Dalibard and C. Cohen-Tannoudji, *J. Opt. Soc. Am. B* **6**, 2023 - 2045 (1989)
- [3] K. Petsas, A. Coates, and G. Grynberg, *Phy. Rev. A* **50**, 5173 - 5189 (1994)
- [4] L. Sanchez-Palencia and G. Grynberg, *Phy. Rev. A* **68**, 023404 (1 - 8) (2003)
- [5] D. Cubero, arXiv:2208.08206 (2022)
- [6] J.-Y. Courtois, S. Guibal, D. Meacher, P. Verkerk, and G. Grynberg, *Phy. Rev. Lett.* **77**, 40 (1996)
- [7] L. Sanchez-Palencia, F. Carminati, M. Schiavoni, F. Renzoni, and G. Grynberg, *Phy. Rev. Lett.* **88**, 133903 (2002)
- [8] M. Schiavoni, F. Carminati, L. Sanchez-Palencia, F. Renzoni and G. Grynberg, *Europhy. Lett.* **59** (4), 493 (2002)
- [9] Equations (44) and (111) in Ref. [1].
- [10] J.-Y. Courtois, in *Coherent and Collective Interactions of Particles and Radiation Beams*, Proceedings of the International School of Physics “Enrico Fermi”, Course CXXXI, edited by A. Aspect, W. Barletta, and R. Bonifacio, 341 - 369 (1995)
- [11] F.-R. Carminati, L. Sanchez-Palencia, M. Schiavoni, F. Renzoni, and G. Grynberg, *Phy. Rev. Lett.* **90**, 043901 (1 - 4) (2003)